C. R. Chimie 19 (2016) 955–962

Contents lists available at ScienceDirect

Comptes Rendus Chimie

www.sciencedirect.com

Full paper/Mémoire

A study on the structure and catalytic performance of $Zn_xCu_{1-x}Al_2O_4$ catalysts synthesized by the solution combustion method for the esterification reaction

Mojgan Hashemzehi, Naser Saghatoleslami, Hamed Nayebzadeh*

Department of Chemical Engineering, Faculty of Engineering, Ferdowsi University of Mashhad, Mashhad, Iran

ARTICLE INFO

Article history:
Received 12 January 2016
Accepted 9 May 2016
Available online 11 June 2016

Keywords:
Microwave-assisted solution combustion (MSC)
Spinel oxide
Alumina
Copper oxide
Esterification
Biodiesel

ABSTRACT

A $Zn_xCu_{1-x}Al_2O_4$ catalyst was prepared via the microwave-assisted solution combustion method (MSC). This method presents a fast procedure for industrial scale catalyst preparation. The physicochemical properties of the fabricated catalyst were characterized using XRD, FTIR, BET, SEM and TEM analyses. The catalytic performance through the esterification reaction was examined under the following conditions: reaction temperature = 180 °C, catalyst concentration = 3% (w/w), molar ratio of oleic acid to methanol = 9 and reaction time = 6 h. XRD results showed that loading both zinc and copper oxides on alumina at a ratio of amounts that were nearly the same resulted in decreased crystalline size and well-dispersed copper-alumina and zinc-alumina crystals. Moreover, the mean pore diameter of the sample was increased by simultaneous loading of zinc and copper oxides on alumina that enhanced permeation of the reactants within pores and increased the interaction of the reactant with the catalyst active sites. The catalyst showed minimum tendency towards adsorbing moisture from air, which was attributed to it having less atoms on the surface through which binding with H_2O molecules takes place. The highest level of activity in the esterification reaction (96.9%) was obtained at the optimum ratio of the Zn:Cu molar ratio, identified to be 2:3. The sample particles ranged from 10 to 30 nm in size, without agglomeration.

1. Introduction

Energy consumption across the globe is currently escalating and this has brought about two important crises: firstly, the problem of carbon emissions in the form of greenhouse gases and secondly, the predicted termination of fossil fuel resources. Scholars have suggested that global temperature could be brought under control by 2100 if there is a sharp reduction of fossil fuel consumption but that a failure to take such an appropriate action could result in irreparable damage to earth. Accordingly, researchers have attempted to enhance renewable and less polluting energy resources to substitute existing systems [1–3]. Biodiesel has been nominated as an appropriate source of energy due to its obvious advantages such as low level pollution, renewable availability, and biological analyzability, and that it can be used in existing engines [4,5]. Biodiesel is generally fabricated from edible oil, inedible oil or animal fat. However, due to the high price of cooking oil for biodiesel production [6], inedible oils such as Jatropha [7], algae [8], and waste cooking oil [9] have often been nominated as suitable alternatives. Biodiesel is usually produced by trans esterification, using triglycerides with short chain alcohols by homogeneous base catalysts such as NaOH or KOH [10]. However, inedible oils contain large amounts of free fatty acids (FFAs) that tend to react with a homogeneous base catalyst to form soap. Subsequently,

* Corresponding author.
E-mail address: h.nayebzadeh@yahoo.com (H. Nayebzadeh).

http://dx.doi.org/10.1016/j.crci.2016.05.006
1631-0748/

separation of soap and a homogeneous catalyst from biodiesel would increase production costs. Researchers have suggested esterifying the FFA before the transesterification reaction. Esterification of FFAs with alcohol is usually performed in the presence of a homogeneous acid catalyst (see Fig. 1) such as H_2SO_4, in a process that produces toxic wastewater that is extremely harmful to the environment. As a result, heterogeneous catalysts have been suggested due to low cost, simple separation process, reusability and environmental reasons [6]. Homogenous catalysts are capable of converting FEAs and triglycerides.

Alumina has received much attention recently as an appropriate catalyst for such purposes due to its high dispersion properties; thermal and chemical stability at high temperature and relatively affordable price. However, due to low activity of alumina in biodiesel production, it serves as a support on which various elements are loaded to increase activity [11,12]. Zinc is an element that has received attention for its unique characteristics such as antibacterial, antifungal and UV filtering properties, as well as high catalytic and photochemical activity [13,14]. Reinoso et al., [15] studied the activity of zinc carboxylic (ZC) salts (as a catalyst) in esterification of oleic acid. A ZC sample was difficult to synthesize in an alcoholic solution for 12 h and showed moderate activity (60%) in the conversion of oleic acid (OA) to the corresponding ester under the conditions of 140 °C, 6 wt.% of catalyst, and 30 molar ratios of OA/methanol. Esterification of OA with methanol was also tested using layered heterogeneous catalysts [16]. Galen et al., [17] utilized ZC salts to produce biodiesel, and tests showed a conversion rate of 60% was achieved after 2 h at 140 °C. Zinc hydroxyl acetate (ZHA) salts exhibited higher level esterification activity of OA compared to zinc hydroxyl nitrate (ZHN).

Other metal oxides have also been loaded on alumina to produce biodiesel. Sanakarnarian et al., [18] examined the activity of various types of spinel alumina ($CuAl_2O_4$, $NiAl_2O_4$, $CoAl_2O_4$ and $ZnAl_2O_4$) on biodiesel production. Tests suggest that copper-alumina and zinc-alumina catalysts demonstrated higher-level activity than other catalysts. Accordingly, as an appropriate transition, metal oxide like copper oxide and zinc oxide (with high thermal conductivity) can be used to improve the activity of alumina.

Various methods are available to synthesis heterogeneous catalysts such as co-precipitation [19], impregnation [20], solvothermal [21] and sol-gel [22] methods. However such methods are problematic according to conditions such as the necessity for continuous pH control, the long length of time needed for synthesis, use of expensive reactants and lack of the required chemical compounds. The method of solution combustion has been presented recently for nano-catalyst production at minimum cost and time inputs and accurate stoichiometric ratios. This method was chosen due to its ability to generate a high temperature during catalyst preparation and without impurity in the synthesized powder product. The solution combustion synthesis method is initiated by an exothermic reaction and it continues with an unabated reaction at elevated temperatures (provided by an external heat source).

The preliminary heat can be provided by an electric spark or by a furnace or microwave. Application of microwave is completely different from other prevalent heating methods in which heat is generated through the interaction of the electromagnetic waves (produced by the source) and the material, whereas in methods such as the furnace method, heat is produced directly by the source. Furthermore, a microwave heat material at the molecular level provides more uniform heating that greatly affects the characteristics of the resultant nano-catalyst [23].

In the present study, $Zn_xCu_{(1-x)}Al_2O_4$ ($x = 1$, 0.8, 0.6, 0.4, 0.2, and 0) catalysts were synthesized by the MSC method, and optimum amounts of copper and zinc oxides for loading on alumina were determined. Then, the characteristics of the catalyst were determined by XRD, FTIR, BET, SEM, and TEM analyses and the obtained results were discussed. Finally, the activity of each catalyst during the esterification reaction was examined.

2. Experiment

2.1. Materials and catalyst preparation

Copper, zinc, aluminum nitrates (as the oxidizer), and urea (as the fuel) for the synthesis of catalysts by the MSC method were obtained from Merck Co. (Germany). Urea served as the fuel, due to it being cheap, readily-available and able to create a high temperature [24]. Aluminum nitrate, together with appropriate molar ratios of copper nitrate and zinc nitrate was dissolved in a minimum volume of water to prepare $Zn_xCu_{(1-x)}Al_2O_4$, where $x = 1$, 0.8, 0.6, 0.4, 0.2, and 0; the produced compounds were labelled ZA, 0.8ZCA, 0.6ZCA, 0.4ZCA, 0.2ZCA, and CA, respectively. Then, a specified amount of urea (determined by thermochemistry and combustion principles) was added to the solution. The resultant solution was then mixed by using a magnetic stirrer at 400 rpm at 80 °C. A clear viscous gel was obtained

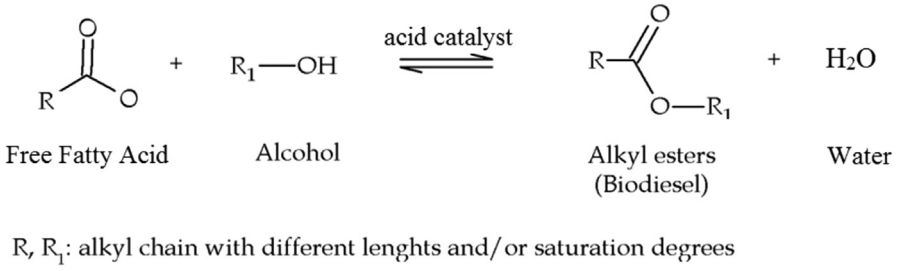

Fig. 1. Schematic of the esterification reaction.

once the water content had evaporated. The gel was subsequently placed into a microwave oven operating at its highest power (Daewoo, KOC9N2TB, 900 watts). Accordingly, the remaining water was evaporated and the residual material enflamed, much fume was given off as the urea started burning. After 5 min of irradiation, a foamy catalyst was synthesized.

As suggested by Jain et al. [25], calculating an appropriate fuel-to-oxidizer ratio is of considerable importance for sample synthesis. This method examines all pertinent elements to the oxidizer to calculate the ratio, regardless of whether the element is in the chemical structure of nitrates (oxidizers) or fuel (reducer). For instance, in the current study, oxygen was considered as the oxidizer with hydrogen, aluminum, copper, and zinc taken as reducers. Moreover, nitrogen was used as the inert element. In this method, elements were loaded according to valence: oxygen (−2), hydrogen (+1), aluminum (+3), zinc (+2), and nitrogen (0). Therefore, equivalent capacity for aluminum nitrate, zinc nitrate and urea was found to be −15, −10, and +6, respectively [26]. However, in most cases, researchers have suggested the application of the stoichiometric ratio of the oxidizer to reducer, as the ratio has an affect on the characteristics of the produced powder [27]. Indeed, the application of a lower ratio has resulted in the formation of amorphous materials, whereas a fuel-rich mixture gives rise to an agglomerated structure. In this case, the amount of fuel was determined by setting the oxidizer-to-reducer stoichiometric ratio to 1. It is noteworthy that under conditions of the lowest reducing power (total valence = 6), urea produces the lowest volume of gas. The ratio of metal nitrate capacity to urea capacity determined the number of moles of urea. For example, in order to calculate the parameter of $Zn_xCu_{1-x}Al_2O_4$, the following calculations should be carried out.

$$x\,Zn(NO_3)_2\cdot 6H_2O + (1-x)Cu(NO_3)_2\cdot 6H_2O + 2\,Al(NO_3)_3\cdot 9H_2O + Y\,CO(NH_2)_2 \rightarrow Zn_xCu_{1-x}Al_2O_4 + Y\,CO_2 + (Y+4)N_2 + (24+(2\times Y))H_2O \quad (1)$$

$$Y = [(-10)+(2\times(-15))]/6 = 6.67 \quad (2)$$

2.2. Catalyst characterization

In order to recognize the phases and crystalline size of the catalysts, X-ray diffraction (XRD) analysis was performed using an UNISANTIS/XMP 300 in the range of 20–70 degree at a scan speed of 10 degrees per minute. Furthermore, a SHIMADZU 4300 (Japan) was utilized to capture FT-IR spectra in the range of 400–4000 cm^{-1}. Measurements of the pore diameter, porosity and surface area of each catalyst were taken via the BET method utilizing a Belsorp mini II1 (Japan). Evaluations of surface acidity and acid strength of the catalyst were carried out by titrating with n-butylamine (0.01 N) using the so-called Hammett indicators: methyl red (4.8), methyl orange (3.3) and violet crystal (0.8). The acid strength is reportedly stronger than the weakest indicator that exhibits a colour change and weaker than the strongest indicator that produces no colour change. Acidity was calculated in mole of acid sites per gram of catalyst and acidity strength was expressed in terms of the Hammett acidity (H_0). Note that, titration by using *n*-butylamine allows for the measurement of the number of acid centers (mmol/g) having an H_0 equal to/or lower than the pK_a value of the indicator. Water stability of the solid acid catalysts, expressed as mmole of NaOH consumed per gram of catalyst, was estimated by titrating a solution of 0.2 g of catalyst in 10 ml of deionized water stirred vigorously for 1 h using 0.1 M NaOH solution. In addition, Scanning Electron Microscopy (HITACHI S4160) was used to investigate the morphology of the nano-catalyst. Finally, Transmission Electron Microscopy (TEM) (LEO 912AB) was utilized to assess the catalyst in terms of the rate of activity in relation to the particle size.

2.3. Catalyst testing

The activity of the fabricated catalysts was discussed in the esterification reaction of OA to the corresponding methyl ester form. This reaction was conducted in a batch system composed of an 80 ml stainless steel reactor; the reactor was operated at 180 ± 3 °C (set by using a type K thermocouple) for 6 h. The molar ratio of methanol to oleic acid was about 9, and the weight percent of the catalyst was 3 wt.% with a fixed stirring speed of 600 rpm. Once the reaction had completed, the obtained mixture was filtered to remove the catalyst. The biodiesel was then heated to 80 °C and held for 90 min to eliminate water and any extra methanol content. The yield of conversion of OA to methyl ester was calculated based on acidity reduction of OA by the standard titration method using potassium hydroxide [28].

3. Results and discussion

3.1. X-ray diffraction (XRD)

Fig. 2 shows the results of XRD analysis of alumina loaded by different molar ratios of zinc and copper oxide. No change was seen in the positions of peaks that confirmed the cubic structure of the crystallite of all samples. According to Fig. 2a, peaks at 31.3, 36.8, 55.7, 59.3, and 65.2° can be attributed to the formation of the spinel type zinc aluminate crystal [29]. However, only peaks of copper oxide were visible for CA (Fig. 2f), illustrating low reaction temperature during combustion. Yanyan et al., [30] reported that the temperature of the catalyst preparation medium should be increased to 800 °C to achieve pure $CuAl_2O_4$. The weak peak at $2\theta \approx 50°$ may correspond to the spinel type copper aluminate. The copper oxide peak at 38° overlapped other peaks of zinc-alumina spinel at 31.3 and 36.8°. Fig. 2e shows that all peaks related to copper oxide and the weak peak at 36.8° corresponded to $ZnAl_2O_4$ spinel.

As shown in Fig. 2d, sample 0.4ZCA exhibited appropriate dispersion of copper oxide and zinc-alumina spinel, confirmed by the peaks of the corresponding height indicating a single-layered structure. This consistency was not observed in other samples. In Fig. 2c and b (related to samples 0.6ZCA and 0.8ZCA, respectively), the dispersion level was the same as that of zinc aluminate, except that

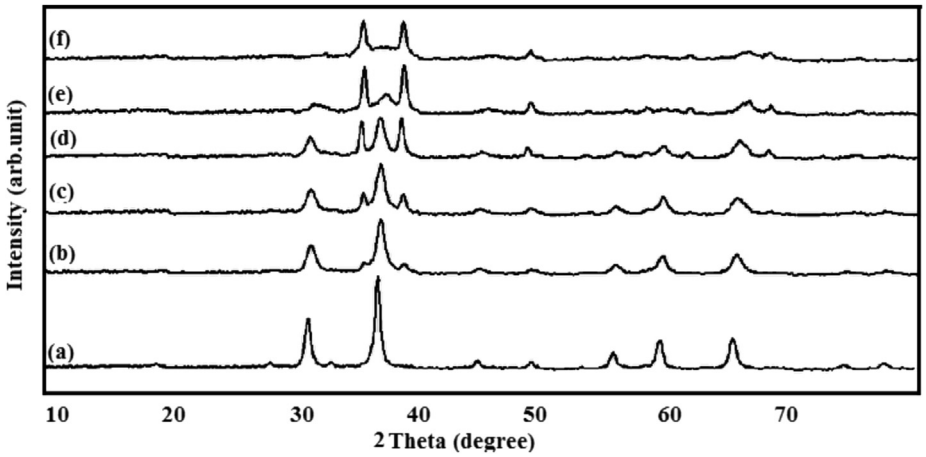

Fig. 2. The XRD patterns of (a) ZA, (b) 0.8ZCA, (c) 0.6ZCA, (d) 0.4ZCA, (e) 0.2ZCA, and (f) CA.

weak peaks at 34 and 38° corresponded to copper oxide. None of the XRD patterns indicated an alumina crystal, revealing well-dispersed alumina within the nano-catalyst. Moreover, the characteristic peaks of ZA spinel were weakened according to an increased amount of doped Cu, indicating that doping Cu reduced the crystallinity of the catalyst [20]. Obtained through the application of the Scherrer equation, the average crystallite sizes of ZA, 0.8ZCA, 0.6ZCA, 0.4ZCA, 0.2ZCA and CA were calculated to be 12, 11, 10, 8, 12, and 16 nm, respectively. In fact, temperature was considered as an important factor for crystal growth of components. The researchers report that lower enthalpy of formation can be attributed to higher temperature during material synthesis, resulting in less crystal formation [31].

3.2. FTIR study

FTIR spectra of nano-catalysts are illustrated in Fig. 3. As seen in the figure, the characteristic peaks corresponding to frequencies of metal oxides were of similar frequency range in all samples, because the atomic mass of copper is roughly equal to that of zinc. Fig. 3a shows the vibration peak of Zn–O at 492 cm^{-1} related to octahedral metal stretching and intrinsic stretching vibrations of metal at the tetrahedral sites at 557 and 668 cm^{-1} [23,32]. In Fig. 3f, the broad bond at 883 cm^{-1} was probably related to copper oxide [33]. When both copper oxide and zinc oxide were loaded on alumina, copper oxide bonds overlapped the zinc oxide bonds. Furthermore, the peak at 1388 cm^{-1} related to nitrate anions (as seen in Fig. 3a and f) was not observed in 0.4ZCA. This demonstrates more complete reactions during 0.4ZCA synthesis. In all samples, the broad peaks at 3000–3500 cm^{-1} and 1600 cm^{-1} were associated with the O–H stretching vibration of water molecules and flexural vibration bonds (O–H), respectively [34]. Indeed, such bonds were due to the hydrophilic characteristics of catalysts to moisture content in air. The minimum bonding level belongs to the sample 0.4ZCA, proving that this nano-catalyst had minimum tendency toward adsorbing

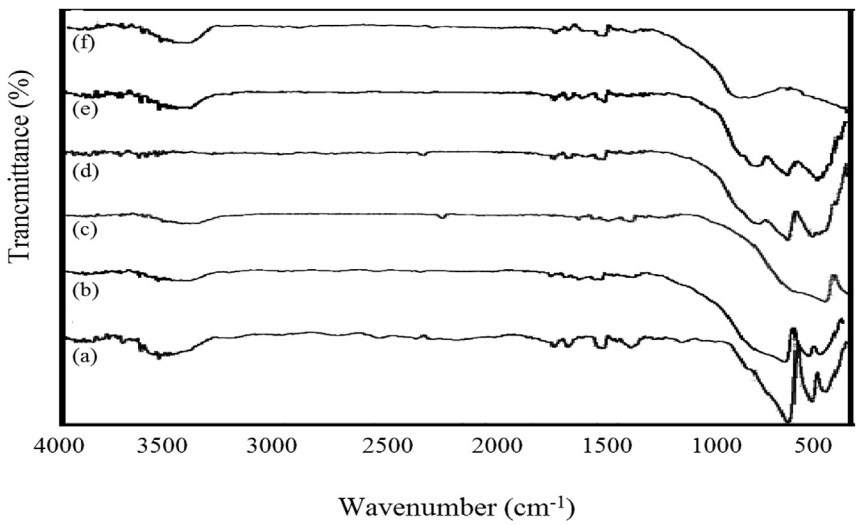

Fig. 3. FTIR spectra of (a) ZA, (b) 0.8ZCA, (c) 0.6ZCA, (d) 0.4ZCA, (e) 0.2ZCA, and (f) CA.

moisture from air, owing to the lower number of atoms on the surface for binding with H_2O molecules [35].

3.3. BET and BJH analysis

Fig. 4 shows the absorption-desorption isotherm at −196 °C for different nano-catalysts. According to these results, all samples showed type IV pattern with different forms of hysteresis loops based on the Brunauer, Deming, Deming and Teller (BDDT) classification. The composition of the isotherm curve and width of the hysteresis loop supply important information on the textural characteristics of nano-catalysts. When zinc was solely loaded on alumina, the formed pores were column shaped, but they were cylindrical in other samples. Two parallel lines were observed in these samples indicating that cavities had the same radii. The hysteresis loop was closed at relative pressure in the range of 0.8–1, which proves the existence of large mesopores. It is noteworthy that the hysteresis loop curve is related to the consistency in pore diameter. Inset diagrams in Fig. 4 indicate pore diameter distribution in the range of 1.5 to 15 nm.

Table 1
BET surface area, pore volume and mean pore size of the samples.

Sample	Surface area (m^2/g)	Pore volume (cc/g)	Mean pore size (nm)
ZA	45.35	0.08	7.12
0.8ZCA	1.64	0.02	5.82
0.6ZCA	1.01	0.02	7.41
0.4ZCA	5.12	0.01	8.64
0.2ZCA	7.09	0.01	7.61
CA	23.70	0.03	4.79

Reaction conditions: 180 °C, molar ratio of methanol/OA: 9, catalyst concentration: 3 wt.%, reaction time: 6 h.

The BET surface area, pore diameter and pore volume of samples are listed in Table 1. As shown, ZA and CA catalysts had the maximum surface area. This surface area exhibited a drastic reduction when the mixture of zinc and copper was loaded on alumina. XRD analysis shows that the crystallite diameter of zinc aluminate spinel decreased with increase in copper, even in a small quantity; such that the copper crystals probably found a route into the pores where they tended to strongly reduce the availability of active sites in the sample. Simultaneous loading of zinc

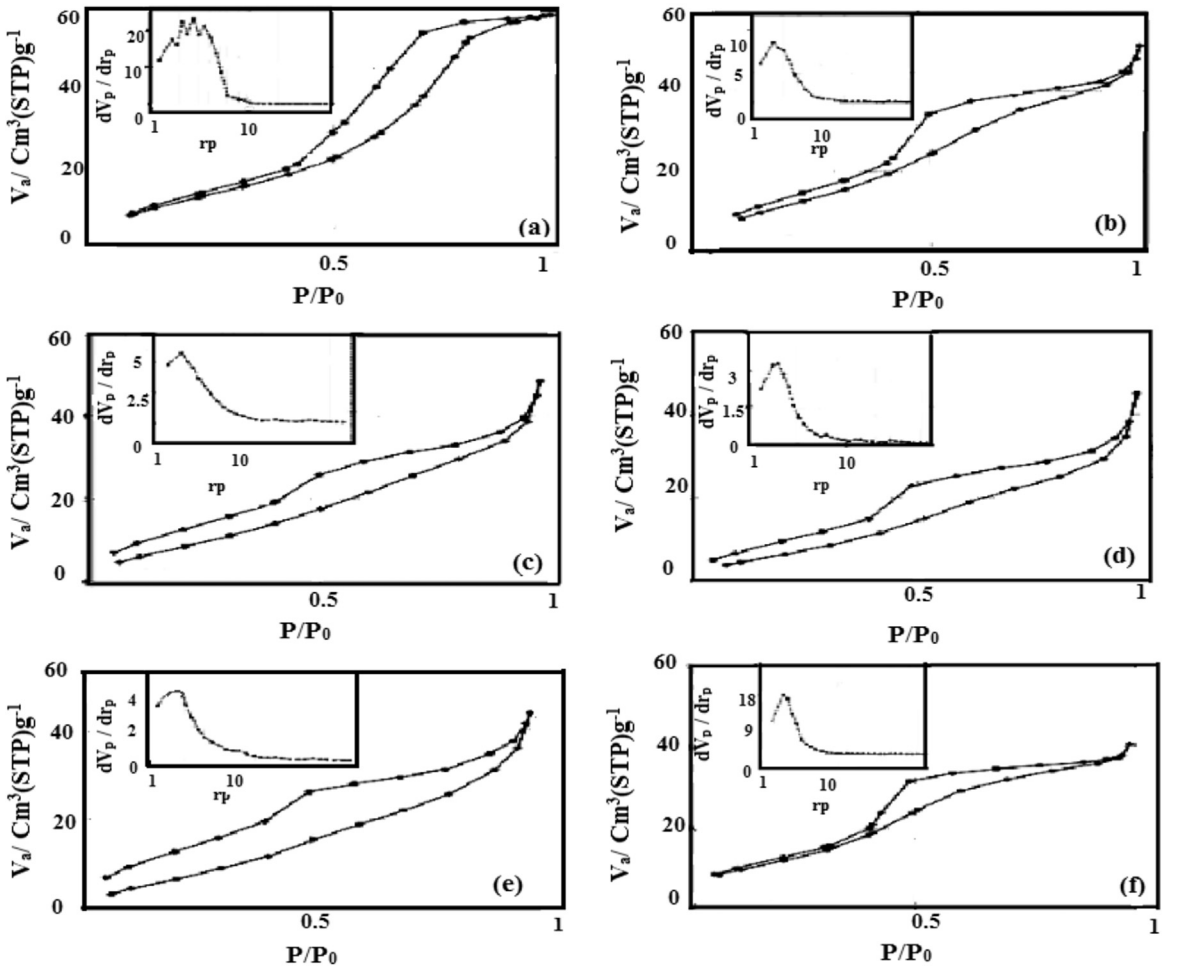

Fig. 4. Hysteresis loops of the N_2 adsorption-desorption isotherm (inset: BJH pore size distribution) for (a) ZA, (b) 0.8ZCA, (c) 0.6ZCA, (d) 0.4ZCA, (e) 0.2ZCA, and (f) CA.

oxide and copper oxide on alumina increased pore diameter facilitating permeation of FFAs into pores of the nano-catalyst, which enhanced the connection of FFAs to active acidic sites of the nano-catalyst. When the Zn/Cu ratio was decreased for loading on alumina, bigger crystals were formed due to the higher temperature during combustion. Consequently, when urea burned at higher combustion temperature, large amounts of gas were released very rapidly that resulted in significantly increased pore diameter. The 0.4ZCA catalyst showed the largest pore diameter that minimized limitation on the diffusion of large OA molecules into the catalyst pores.

It is worth noting that catalyst activity is not dependent only on the surface area. Jacobson et al. [36] reported that solid nano-catalysts should have pore diameter appropriate to permeate triglyceride or FFA molecules. Granados et al., [37] reported that the diameter of methyl oleate (ester form of OA) is about 2.5 nm. A number of studies have emphasized that restricted diffusion transpires when reactant molecules and pores have comparable dimensions. For a narrow-pore catalyst (mean pore diameter $\approx$ 4 nm), a 50% decrease in catalytic activity relative to the activity of catalysts with medium ($d \approx 6$ nm) or wide ($d \approx 8$ nm) pore size can be expected [38]. Higher amounts of copper oxide (Cu/Zn ratio of 4) were the result of decreasing pore diameter, while the surface area was increased. This caused agglomeration of particles on the surface of the catalyst. Therefore, the 0.4ZCA catalyst with maximum pore diameter was considered to be the most preferable selection as the catalyst for application in further studies.

3.4. Acid strength, acidity, activity and reusability of the catalyst

Water stability, acidity and activity properties of the synthesized nano-catalysts are listed in Table 2. As seen in the table, acid strength of all samples was in the range of 0.8 to 3.3, as obtained by Hammett indicators. In addition, it was clearly observed that the activity of samples increased with increased CuO. However, as further copper oxide (i.e. over a molar ratio of 0.6) was loaded on alumina, acidity was extremely decreased due to agglomeration of CuO on the surface of zinc aluminate spinel that covered the acid sites of zinc aluminate. Acid sites of a catalyst are known to have an important role in the esterification reaction. According to the results of XRD analysis, the 0.4ZCA catalyst showed broad peaks with low intensity compared to the other samples, confirming good dispersion of copper and zinc oxides on alumina and an intense interaction, resulting in higher catalytic activity [39]. The 0.4ZCA catalyst showed maximum catalytic activity with relatively low water solubility. This is an important factor in the esterification reaction where water is the by-product. Therefore, 0.4ZCA can significantly address some drawbacks of common materials used as catalysts or as a support in industrial esterification processing.

Table 2
Acidic and catalytic activity properties of the samples.

Sample	Acid strength	Acidity (mmol/g)	Water stability (mmol/g)	Conversion (%)
ZA	$3.3 < H_0 < 0.8$	0.304	0.087	94.4
0.8ZCA	$3.3 < H_0 < 0.8$	0.322	0.099	94.7
0.6ZCA	$3.3 < H_0 < 0.8$	0.365	0.095	95.5
0.4ZCA	$3.3 < H_0 < 0.8$	0.386	0.086	96.9
0.2ZCA	$3.3 < H_0 < 0.8$	0.299	0.099	94.0
CA	$3.3 < H_0 < 0.8$	0.211	0.105	90.2

3.5. Scanning electron microscopy (SEM)

Fig. 5 shows the SEM images of ZA, 0.4ZCA and CA. Results show the distribution of particles with specified boundaries and formation of good porosity within the sample. Fig. 5a demonstrates the formation of zinc aluminate particles accompanied by agglomeration of nano-catalysts, indicative of solution combustion synthesis. SEM images show that the morphology of 0.4ZCA was different from that of pure ZA and CA. It was indicated that the surface of the sample consisted of sporadic and irregular spherical nanoparticles that were properly crystallized, while no agglomeration was observed.

Sufficient heat of formation during synthesis of the catalyst made a dense, closely packed array of nanoparticles with well-defined borders. The SEM image of copper-alumina showed that the catalyst constituted a mesoporous surface that was probably due to the release of large volumes of gas during combustion. Moreover, spherical particles of copper oxide were formed with no agglomeration (Fig. 5c).

3.6. Transmission electron microscopy (TEM)

TEM analysis was conducted to investigate the catalyst particle size and agglomeration status. Fig. 6 shows TEM images of 0.4ZCA as the most active catalyst for the esterification reaction. As seen in the figure, the particle size ranged from 10 to 30 nm and particles were irregular in structure. Also, particle distribution and size were not uniform and no agglomeration tendency was observed.

3.7. Comparison with the literature

Various types of heterogeneous catalysts (including zinc, copper and alumina) were utilized for biodiesel production, as shown in Table 3. These catalysts were synthesized by different methods and biodiesel was produced under different sets of reaction conditions. The chemical methods used in most other studies for preparing catalysts take a long time (over 48 h) and require heat treatment (calcination) to produce the desired catalyst. But in this study, a mixed zinc-copper aluminate catalyst was synthesized by the MSC method in 5 min, indicating good potential of the method to produce industrial scale biodiesel. The produced catalyst showed high activity in the esterification reaction due to its large surface area and large pore size. Moreover, the catalyst obtained by microwave irradiation had good pore size distribution (see Fig. 4). This was the result of uniform heating by microwave irradiation on a molecular scale. Therefore, the catalyst prepared in the present study showed higher level activity compared to

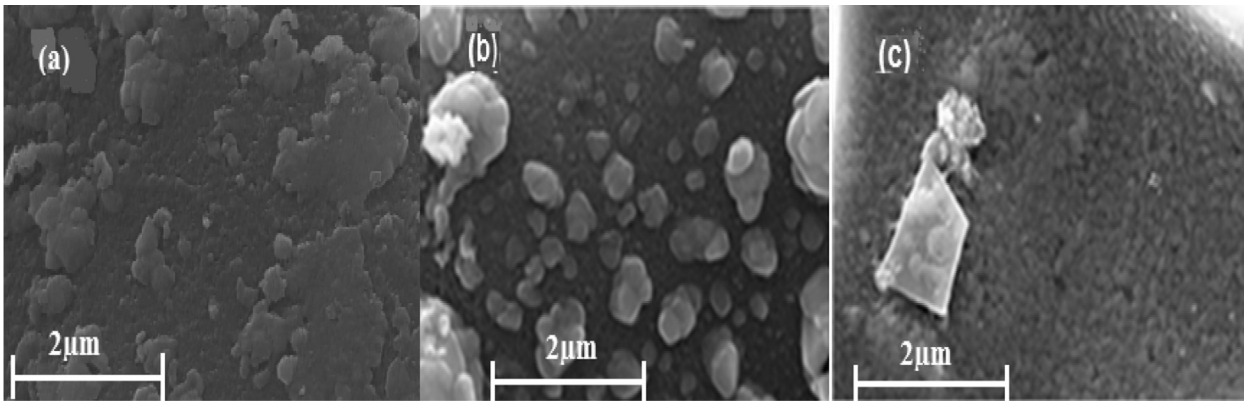

Fig. 5. SEM images of catalysts: (a) ZA, (b) 0.4ZCA, and (c) CA.

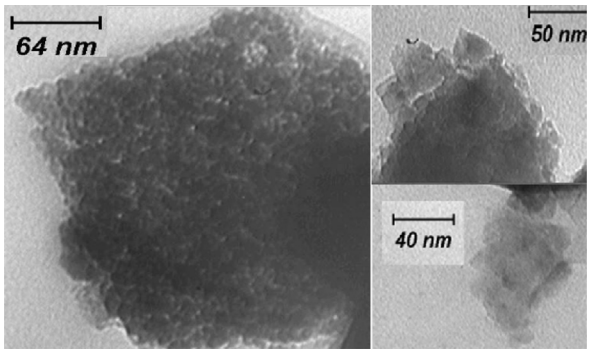

Fig. 6. TEM image of 0.4ZCA.

those prepared by conventional solution combustion methods, as reported by Coutinho et al., [38].

Exhausting huge amounts of gases in the course of catalyst synthesis (which moderates the reaction conditions), the MSC method can provide a mesoporous catalyst of large surface area and mean pore size. Moreover, high temperature during catalyst preparation determines that the catalyst provides high stability against water solubility, deactivation or degradation in the presence of extreme reaction temperature. Therefore, nano-scale catalysts prepared by the MSC method can be recommended with confidence as catalysts to support and/or promote industrial processes.

4. Conclusion

A series of nano-catalysts of the general formula $Zn_xCu_{(1-x)}Al_2O_4$ ($x = 1, 0.8, 0.6, 0.4, 0.2, 0$) were synthesized successfully using the method of microwave-assisted solution. Data collected from XRD, FTIR, BET, SEM, and TEM analyses showed that the nano-catalyst crystallite size ranged from 7 to 16 nm. Simultaneous loading of zinc and copper oxides on alumina reduced intensity of the peaks, implying better dispersion of particles and interaction between copper-alumina and zinc-alumina. Moreover, simultaneous loading of these oxides caused a drastic increase in pore diameter. In fact, the mean pore diameter of ZA/CA was enlarged by simultaneous loading of both zinc and copper oxides on alumina, resulting in improved activity of 0.2ZCA, 0.4ZCA, 0.6ZCA, and 0.8ZCA catalysts compared to ZA and CA. Also, the effect of different ratios of

Table 3
List of similar heterogonous catalysts for biodiesel production.

Catalyst	Reaction	CPM[c]	Temp °C	MOR[d]	Catalyst Wt.%	Reaction time (h)	Yield (%)	Ref
0.4ZCA	E[a]	MSC	180	9	3	6	96.9	
Zinc acetate	E	Purchased	220	4	1	1	60	[40]
ZnO/Zeolite	E	HIP[b]	160	–	5	6.6	90	[41]
ZHA[e]	E	Precipitation	140	30	3	2	87	[16]
$ZnAl_2O_4$	E	SCM[f]	160	4	5	1	38	[42]
KF/Zn(Al)O	T[g]	HIP	140	6	3	1	95	[41]
$Zr/ZnAl_2O_4$	T	Co-precipitation	140	20	4	1	91.7	[20]
CuVOP[h]	T	Hydrothermal	65	6.75	1.5	62.5 h	65	[43]
Cu–Mg–Al	T	Co-precipitation	65	10	7.5	48	67.4	[44]

[a] E: Esterification.
[b] HIP: Hydrothermal Impregnation Precipitation.
[c] CPM: Catalyst Preparation Method.
[d] MOR: Methanol-to-oil ratio.
[e] Zinc Hydroxyl acetate.
[f] SCM: Solution Combustion Method.
[g] T: Transesterification.
[h] Copper vanadium phosphate.

Zn/Cu on catalytic performance (in terms of biodiesel production) was investigated and the 0.4ZCA catalyst exhibited the best activity. A yield of 96.93% was obtained for the esterification reaction. Based on these results, the solution combustion method is recommended as a very effective and useful method to synthesize a stable catalyst with good activity and within a short time, such that the method can be applied to industrial scale catalyst production.

Acknowledgements

The authors gratefully acknowledge the financial support of the Iran Nanotechnology Initiative Council (74670).

References

[1] M.Y. Koh, T.I.M. Ghazi, Renew. Sust. Energy. Rev. 15 (2011) 2240.
[2] P.-q. Tan, Z.-y. Hu, D.-m. Lou, Z.-j. Li, Energy 39 (2012) 356–362.
[3] N. Mrad, E.G. Varuvel, M. Tazerout, F. Aloui, Energy 44 (2012) 955.
[4] J.-H. Ng, H.K. Ng, S. Gan, Appl. Energy 90 (2012) 58.
[5] H. How, Y. Teoh, H. Masjuki, M. Kalam, Energy 48 (2012) 500.
[6] H.E. Hoydonckx, D.E. De Vos, S.A. Chavan, P.A. Jacobs, Top. Catal. 27 (2004) 83.
[7] P. Goyal, M. Sharma, S. Jain, J. Pet. Sci. Res. (2012).
[8] A. Demirbas, M.F. Demirbas, Energy. Convers. Manage 52 (2011) 163.
[9] A. Talebian-Kiakalaieh, N.A.S. Amin, H. Mazaheri, Appl. Energy 104 (2013) 683–710.
[10] F. Ma, M.A. Hanna, Bioresour. Technol. 70 (1999) 1.
[11] G. Busca, Adv. Catal. 57 (2014) 319.
[12] M. Álvarez, M.J. Ortiz, J.L. Ropero, M.E. Niño, R. Rayon, F. Tzompantzi, R. Gomez, Chem. Eng. Commun. 196 (2009) 1152.
[13] C. Jayaseelan, A.A. Rahuman, A.V. Kirthi, S. Marimuthu, T. Santhoshkumar, A. Bagavan, K. Gaurav, L. Karthik, K.B. Rao, Spectrochim. Acta. Part A. 90 (2012) 78.
[14] K. Kanade, B. Kale, R. Aiyer, B. Das, Mater. Res. Bull. 41 (2006) 590.
[15] D.M. Reinoso, D.E. Damiani, G.M. Tonetto, Appl. Catal. A-Gen. 449 (2012) 88.
[16] D.M. Reinoso, M.B. Fernandez, D.E. Damiani, G.M. Tonetto, Int. J. Low-Carbon. Tech. (2011) ctr040.
[17] G.J. Suppes, M.A. Dasari, E.J. Doskocil, P.J. Mankidy, M.J. Goff, Appl. Catal. A-Gen. 257 (2004) 213.
[18] T. Sankaranarayanan, R.V. Shanthi, K. Thirunavukkarasu, A. Pandurangan, S. Sivasanker, J. Mol, Catal. A-Chem. 379 (2013) 234.
[19] Y. Fan, X. Lu, Y. Ni, H. Zhang, M. Zhu, Y. Li, J. Chen, Appl. Catal. B-Environ. 101 (2011) 606.
[20] Q. Liu, C. Wang, W. Qu, B. Wang, Z. Tian, H. Ma, R. Xu, Catal. Today 234 (2014) 161.
[21] Y. Sarikaya, K. Ada, T. Alemdaroğlu, I.h. Bozdoğan, J. Eur. Ceram. Soc. 22 (2002) 1905.
[22] V.B.R. Boppana, D.J. Doren, R.F. Lobo, Chemsuschem 3 (2010) 814–817.
[23] A. Manikandan, J.J. Vijaya, L.J. Kennedy, M. Bououdina, Ceram. Int. 39 (2013) 5909.
[24] G.K. Reddy, G. Thrimurthulu, B.M. Reddy, Catal. Surv. Asia 13 (2009) 237.
[25] S. Jain, K. Adiga, V.P. Verneker, Combust. Flame. 40 (1981) 71.
[26] I. Ganesh, B. Srinivas, R. Johnson, B. Saha, Y. Mahajan, Brit. Ceram. Trans. 101 (2002) 247.
[27] D. Fumo, M. Morelli, A. Segadaes, Mater. Res. Bull. 31 (1996) 1243.
[28] J. Marchetti, A. Errazu, Fuel 87 (2008) 3477.
[29] C. Alves, A. de Oliveira, S. Carneiro, R. Santos, S.V. de Melo, H. Andrade, F. Marques, E. Torres, Procedia. Eng. 42 (2012) 1928.
[30] J. Yanyan, L. Jinggang, S. Xiaotao, N. Guiling, W. Chengyu, G. Xiumei, J. Sol-Gel. Sci. Technol. 42 (2007) 41.
[31] A. Navrotsky, O. Kleppa, J. Inorg, Nucl. Chem. 30 (1968) 479.
[32] R. Ianoş, R. Lazău, I. Lazău, C. Păcurariu, J. Eur. Ceram. Soc. 32 (2012) 1605.
[33] M. Salavati-Niasari, F. Davar, M. Farhadi, J. Sol-Gel. Sci. Technol. 51 (2009) 48.
[34] G.T. Behnke, K. Nakamoto, Inorg. Chem. 3 (1967) 433.
[35] C. Ragupathi, J.J. Vijaya, S. Narayanan, L.J. Kennedy, S. Ramakrishna, Chinese. J. Catal. 34 (2013) 1951.
[36] K. Jacobson, R. Gopinath, L.C. Meher, A.K. Dalai, Appl. Catal. B-Environ. 85 (2008) 86.
[37] M.L. Granados, M.Z. Poves, D.M. Alonso, R. Mariscal, F.C. Galisteo, R. Moreno-Tost, J. Santamaría, J. Fierro, Appl. Catal. B-Environ. 73 (2007) 317.
[38] I. Lukić, J. Krstić, S. Glišić, D. Jovanović, D. Skala, J. Serb. Chem. Soc. 75 (2010) 789.
[39] H. Fan, H. Zheng, Z. Li, Frontiers. Chem. Eng. China 4 (2010) 445.
[40] C. Song, Y. Qi, T. Deng, X. Hou, Z. Qin, Renew. Energy 35 (2010) 625.
[41] D. Singh, P. Patidar, A. Ganesh, S. Mahajani, Ind. Eng. Chem. Res. 52 (2013) 14776.
[42] J.P. Coutinho, M.C. Silva, S.M.P. Meneghetti, E. Leal, A.C.F. de Melo Costa, N.L. de Freitas, Trans. Tech. Publ. (2012) 1323.
[43] L. Chen, P. Yin, X. Liu, L. Yang, Z. Yu, X. Guo, X. Xin, Energy 36 (2011) 175.
[44] K. Chelladurai, M. Rajamanickam, Int. J. Chem. Tech. Res. 8 (2015) 422.